Distinguishing and quantification of the human visual pathways using high spatial resolution diffusion tensor tractography

Arash Kamali, MD[1], **Khader M. Hasan, PhD**[2,CA], **Pavani Adapa, MD**[3], **Azadeh Razmandi, OD**, **Zafer Keser, MD**[4], **John Lincoln, MD, PhD, MD**[4], and **Larry A. Kramer, MD**[2]

[1]Department of Diagnostic Radiology, University of Medicine and Dentistry of New Jersey Cooper, Camden, New Jersey, USA

[2]Department of Diagnostic & Interventional Imaging, University of Texas at Houston, Houston, Texas, USA

[3]Department of Diagnostic Radiology, University of Nebraska, Omaha, Nebraska, USA

[4]Department of Physical Medicine and Rehabilitation, University of Texas at Houston and TIRR Memorial Hermann NeuroRecovery Research Center, Houston, Texas, USA

[5]Department of Neurology, University of Texas at Houston, Houston, Texas, USA

Abstract

Quantification of the living human visual system using MRI methods has been challenging, but several applications demand a reliable and time-efficient data acquisition protocol. In this study, we demonstrate the utility of high spatial resolution diffusion tensor fiber tractography (DTT) in reconstructing and quantifying the human visual pathways. Five healthy males, age range 24–37 years, were studied after approval of the Institutional Review Board (IRB) at The University of Texas Health Science Center at Houston. We acquired diffusion tensor imaging (DTI) data with 1-mm slice thickness on a 3.0 Tesla clinical MRI scanner and analyzed the data using DTT with the fiber assignment by continuous tractography (FACT) algorithm. By utilizing the high spatial resolution DTI protocol with FACT algorithm, we were able to reconstruct and quantify bilateral optic pathways including the optic chiasm, optic tract, optic radiations free of contamination from neighboring white matter tracts.

CACorresponding Author: Khader M. Hasan, Ph.D., Associate Professor of Diagnostic and Interventional Imaging, Department of Diagnostic and Interventional Imaging, University of Texas Health Science Center at Houston, 6431 Fannin Street, MSB 2.100, Houston, Texas 77030, Tel: Office (713) 500-7690, Fax: (713) 500-7684, Khader.M.Hasan@uth.tmc.edu.

Keywords

Diffusion tensor imaging; diffusion tensor tractography; high spatial resolution; human visual system; visual pathways; retinogeniculocalcarine tract; optic nerve; optic chiasm; optic tract; optic radiations; calcarine cortex; occipital lobe

1. Introduction

The human visual pathway consists of two neuron chains that traverse the brain anterior-posteriorly in an axial plane. Optic nerve fibers project from the retina to the lateral geniculate nucleus (LGN) of the thalamus via the optic chiasm and optic tracts [1]. From the LGN, fibers emerge as the optic radiation carrying information from the contralateral visual field (geniculocalcarine tract or the geniculostriate pathway) and traverse the retrolenticular portion of the internal capsule on their way to their destination in primary visual cortex in the occipital lobe [2, 3].

Challenges in mapping and progress towards quantification of the entire living human visual pathways or retinogeniculcalcarine tracts are historically documented [1]. In particular, imaging the optic nerve (ON) due to its small volume and tortuous geometry, and the harsh MRI environment surrounding it remains challenging [4].

Early reviews and comparison of acquisition parameters and quantitative results between methods have been provided elsewhere [5, 6, 7, 8]. Diffusion-sensitized MRI methods applied to the human visual pathways have utilized regions-of-interest [9, 10], deterministic [11, 12, 13, 14] and probabilistic tractography [15, 16, 17] on separate components of the visual system including optic nerves [9, 18], optic chiasm [19, 20, 21], optic tracts [10], and optic radiations [11–14] including Meyer loop [7, 8]. Qualitatively, the methods adopted to-date to quantify components of the human visual system using diffusion-weighted imaging were different on several aspects including spin history preparation (i.e. fat, cereprospinal fluid and outer volume suppression), k-space sampling (i.e. conventional spin echo, stimulated echoes, line scan, echo-planar imaging), in addition to differences in spatial resolutions (1mm – 4mm), b-factor (300–1000 s mm^{-2}), signal-to-noise ratio (i.e. diffusion encoding, averaging, main magnetic field B_0), plane of acquisition, and scan time [21].

Diffusion tensor imaging (DTI) methods have been applied to various clinical conditions including ischemic injury of optic pathways [22], multiple sclerosis and optic neuritis [9, 18, 23, 24, 25, 26], neuromyelitis optica [27], diabetes mellitus [28], glaucoma [29, 30, 31], amblyopia [32], blindness [33, 34], cerebral palsy [35], and in neoplastic involvement of optic pathways [36, 37]. Three dimensional (3D) tractography of the entire human visual system might be more useful in preoperative and/or intraoperative neurosurgical planning to preserve structural integrity and avoid visual field defects by mapping the optic radiations [38, 39] as well as for quantitative assessment of visual recovery after surgery [3, 40, 41, 42, 43, 44] or in congenital lesions [45, 46].

Neuroimaging DTI studies of the human visual pathways including the optic tracts, pretectal fibers and those between the deep gray nuclei and cortex have so far been limited due to

inadequate spatial resolution (in-plane and slice thickness 2–5 mm) and poor signal-to-noise ratio (SNR) [46, 47]. The use of large voxel sizes increase partial volume averaging [47, 48, 49] and contamination from neighboring fiber pathways, in particular, the occipito-pontine tract (OPT). Low SNR results in overestimation of anisotropy and increases errors in eigenvector estimation. This leads to inaccurate white matter connections [47, 48, 49] and false positive results which has been a challenge in tracking the optic tracts and the pretectal fibers in particular. The ability to quantify the volume and corresponding diffusion tensor metrics of the optic pathways across the healthy human lifespan and in various aforementioned clinical scenarios would provide objective useful neuroimaging markers for therapy or modeling the neurobiology of injury or plasticity due to age, training, disease, neurotoxins, high-elevation or even microgravity in long space travels [50].

As mentioned above, several prior DTI tractography studies attempted to trace components of the visual tracts [5–8]. Lack of adequate spatial resolution resulted in partial volume averaging and false positive and negative results. Also susceptibility artifacts and limited spatial resolution have been major drawback in the prior DTI studies [4, 21]. These limitations resulted in inability to trace the subcomponents of the optic tract such as the pretectal fibers [6] or anterior aspect of the optic radiation known as the Mayer's loop in the prior DTI tractography studies [38]. Furthermore, to our knowledge, no illustration of the major neighboring fiber pathways of the visual tracts has been demonstrated by prior DTI tractography studies.

DTI acquisition methodology can be improved by sequence optimization with respect to shorter echo time, decreased partial volume averaging effects and reduced geometrical distortions [4, 10, 21]. This will be advantageous to the study of the delicate fibers of the optic pathway in relation to adjacent major white matter fiber tracts such as the posterior thalamic radiation (PTR) or occipito-pontine tract [14]. The aim of this study is to demonstrate the feasibility of delineation and quantification of the human visual system using high resolution diffusion tensor tractography at higher magnetic field strength and the ability to distinguish the visual tracts from major neighboring fiber tracts [48].

2. Subjects and Methods

2.1. Participant Demographics

This work was Institutional Review Board (IRB) approved and complied with the Healthy Insurance Portability and Accounatbility Act (HIPAA). Five right-handed healthy males (age range of 24–37 years) were included in this study and written informed consent was obtained from all the subjects.

2.2. Conventional MRI data acquisition

All MRI studies were performed on a 3 Tesla Philips Intera clinical MRI scanner with a dual quasar gradient system with maximum gradient amplitude 80 mT/m, maximum slew rate 200 mT/m/ms and an eight channel SENSE-compatible head coil (Philips Medical Systems, Best, the Netherlands).

The conventional MRI (cMRI) protocol included axially prescribed 3D spoiled gradient echo imaging (repetition time (TR) = 8 ms; echo time (TE) = 4 ms) with a square field-of-view (FOV) = 256 x 256 mm and a matrix of 256 x 256 pixels. The slice thickness for the MRI sequences was 1.0 mm with 120 contiguous axial slices covering the entire brain from foramen magnum to vertex [51].

2.3. Diffusion-MRI data acquisition

Diffusion-weighted imaging (DWI) data were acquired axially from the same graphically prescribed cMRI volumes using a single-shot multi-slice 2D spin-echo diffusion sensitized and fat-suppressed echo planar imaging (EPI) sequence, with balanced Icosa21 tensor encoding scheme [51]. The b-factor was 500 s/mm^2 and TR/TE = 14,460/60 ms. The spatial coverage for DTI data matched the 3D cMRI spatial coverage (field-of-view = 256 mm x 256 mm and slice thickness/gap/#slices = 1 mm/0 mm/120). The EPI phase encoding used a SENSE k-space undersampling factor of two, with an effective k-space matrix of 112 x 112 and an image matrix after zero-filling of 256 x 256. The acquisition spatial resolution for DTI data was ~ 2.29 x 2.29 x 1 mm and the digitally interpolated spatial resolution after k-space image construction was 1mm x 1mm x 1 mm. The number of b-factor ~ 0 (b_0) magnitude image averages was 4. The DTI acquisition was ~ 7 min and was repeated three times to enhance SNR for a total of 21 min. The selection of the *b*-factor, parallel imaging, TR and TE enabled entire brain coverage using single shot and interleaved EPI. The thin slice acquisition in space and replication of data in time combined with the DTI encoding provided several quality control options to study SNR and partial volume effects [48, 49] on DTI tracking results [52]. The SNR in the non-diffusion weighted data was ~ 26–31.

2.4. White matter fiber tracking

The imaging data in this study were acquired to cover the entire human brain. As the acquisition data was not optimized specifically toward the study of the extracranial portion of the optic nerves, the frontal aspect of the calvarium including the intraorbital portions of the skull were masked during post processing. This prospectively prevented us from performing tractography of the intra-orbital portion of the optic nerves. Fiber tracking was performed using DTI Studio software and based on the FACT algorithm with a fractional anisotropy (FA) threshold of 0.22 and angle threshold of 60°. Two regions-of-interest (ROIs) were applied to obtain each fiber tract and an "AND" operation was performed to include the fibers passing through both of the ROIs [52, 53]. The T1-weighted volumes were co-registered with the DTI-derived maps on all five subjects allowing better characterization of the anatomic landmarks for placement of the ROIs using FA modulated or color-coded principal eigenvector maps [54, 55].

2.4.1. Fiber tracking regions-of-interest—The locations of the ROIs selected for tracing the optic tract (OT) and optic radiation (OR) are demonstrated in Fig. 1. To trace the OT, the first ROI was placed over the optic chiasm in coronal plane. The second ROI was pursued by selecting the anteroposteriorly oriented association fibers (colored in green) shown in the coronal plane passing through the level of the anterior commissure (Fig. 1a). The first ROI for OR was seeded on the red fibers of the thalamus (right to left oriented fibers that loop over the temporal horn of lateral ventricle before turning medially toward

the calcarine sulcus in the occipital lobe). The second ROI for OR was placed on the green fibers (anteroposteriorly oriented fibers) in the occipital cortex (Fig. 1b). We used the ROIs described in prior DTI studies for delineation of the inferior longitudinal fasciculus (ILF), inferior frontooccipital fasciculus (IFOF), PTR [11–14, 56] and occipito-pontine tract (OPT) [57]. For tracing the optic nerve we seeded the first ROI over the optic chiasm in the coronal plane followed by the second ROI selected over the green (anteroposteriorly oriented) fibers of the optic nerve in the coronal plane through the anterior corpus callosum (Fig. 1c). Undesired fiber tracts were excluded using NOT operation [11–14]. The reproducibility of the fibers was confirmed by two of the authors with more than 8 years of experience in DTI tractography (AK, KMH). Given the two seed approach of the ROIs, the fiber tracts were clearly delineable from adjacent pathways. Since the ROI placement was placed with respect to well-identified anatomical landmarks, all results were reproducible by the two raters across all 5 subjects. The description of the ROIs for visual tracts is more clarified in the images and captions.

3. Results

3.1. Tractograms

Representative tractogram of the optic tract is shown in Figs. 2a–2f. We also iluustarate fiber pathways arising from the posterior thalami such as PTR as well as major projection and association fiber tracts coursing adjacent to the OR such as the OPT, ILF and IFOF [12, 13]. The optic radiations are covered by the IFOF and OPT along their course through the occipital white matter can be confused with the ILF (Figs. 3 and 4.). The posterior thalamic radiation (purple fibers in Fig. 4) courses above the optic radiation and projects to the parieto-occipital cortex.

3.1.1. Opticnerve, optic chiasm, optic tract and pretectal fibers of the optic pathways—After decussating in the optic chiasm, the optic nerves continue as the optic tracts (OT) to synapse with the second order neurons of the ipsilateral LGN, pulvinar of the thalamus and superior colliculus (pretectal nuclei) in the midbrain (Fig. 3c). Pretectal fibers are responsible for the pupillary light reflex, smooth pursuits and accommodation reflex [55, 56].

3.1.2 Geniculocalcarine tract or optic radiation—The optic radiation (OR) fibers emerges from the LGN and traverses through the retrolenticular part of the posterior limb of the internal capsule [1, 2, 3]. The OR fibers project to the ipsilateral visual cortex in the occipital lobe adjacent to the calcarine sulcus (yellow fibers in Fig. 3 and 4). Optic radiations on each side has distinctively superior fibers (Baum's loop) coursing dorso-medially through the parietal lobe toward the occipital cortex. Inferior fibers coursing antero-inferiorly around the temporal horn of the lateral ventricle turn medially and posteriorly forming the Meyer's loop [3] before relaying to the lingual gyrus of the calcarine sulcus of the occipital lobe (arrow in Fig. 3a).

3.1.3 Inferior longitudinal fasciculus—The Inferior longitudinal fasciculus (ILF) (blue fibers in Figs. 3 and 4) running laterally and inferiorly above OR is a connection between the temporal and occipital lobes. The ILF overlaps the OR in most of the occipital white

matter. The ILF is spatially overlapped by the inferior fronto-occipital fasciculus (not shown) which runs medially and above the OR.

3.1.4 Inferior fronto-occipital fasciculus (IFOF)—The IFOF (pink fibers in Figs. 3f– 3i) is the longest association pathway of the brain which connects the ipsilateral frontal and occipital lobes. The IFOF merges with the frontal projection of the uncinate fasciculus as well as the frontal projections of the extreme capsule in the frontal lobe. In the occipital lobe, the IFOF overlaps the optic radiation and occipito-pontine tract and all are covered by the inferior longitudinal fasciculus (Fig. 3, 4). Meyer's loop of the OR courses deep to the IFOF throughout its course (Fig. 3g).

3.1.5. Posterior Thalamic Radiation—The posterior thalamic radiation (PTR) fibers arise from the posterior thalamus (pulvinar), course through the retrolenticular part of the posterior limb of internal capsule and insert into the occipital and posterior parietal cortices (purple fibers in Fig. 4f). These projection fibers include the optic radiations but can be separated from the remainder of the OR (yellow fibers in Figs. 2–4) using our high resolution protocol.

3.1.6. Occipito-pontine tract (OPT)—The OPT is part of the corticopontocerebellar pathways [57]. This pathway (green fibers in Figs. 4b and 4c) projects from the occipital cortex to the ipsilateral pontine nuclei via the retrolenticular part of the posterior limb of internal capsule and lateral third of the cerebral peduncle in the midbrain. These fibers are known to be associated with eye pursuit movements and with visual perception.

3.2. Quantitative Results

A quantitative summary of the mean and standard deviation values of the fiber tract volume and corresponding fractional anisotropy and mean diffusivity values of the bilateral ORs and OTs in all the five subjects is provided in Table 1. Our quantitative analysis demonstrates that there is an insignificant trend towards left sided laterality of the FA values of the optic radiations ($p = 0.06$). Note that the fractional anisotropy of pooled right and left OR is comparable to OT ($p = 0.48$). The volume of OR tract is comparable in the two hemispheres ($p = 0.31$).

4. Discussion

Prior DTI studies of the visual pathways used data acquired with axial sections thicker than 1.5 mm. Even with higher SNR at 3T magnetic field strength, visual pathways including the optic tracts and small branches such as the pretectal fibers could not be traced without contamination from neighboring white matter tracts [6, 16]. Because of the larger voxels, though the SNR was enhanced, partial volume averaging was exacerbated which proved detrimental to the mapping of crossing fibers, especially the optic chiasm [6, 16, 19, 20, 21]. Effects of partial volume averaging in DTT due to slice thickness were studied previously in the context of crossing fibers and few attempts were made to quantify the entire human visual pathways [6, 16, 58], especially the optic radiations at high spatial resolution [59].

In MRI, SNR is proportional to the main magnetic field (B_0), voxel volume and square root of the total sampling time [21, 48]. One way to enhance signal intensity in DTI is to increase the main magnetic field strength that can counter the effects of small voxel volume at high spatial resolution. Experimental DTI tractography studies have attempted using 7T and 9T scanners for mapping the optic tracts in primate [60] and human visual systems [21]. DTI sequence optimization with respect to shorter echo time and decreased partial volume averaging effects will be advantageous to study of the optic nerves and optic tracts which are much smaller in volume (i.e. ~ 0.5 mL; [18]) than other projection fibers of the central nervous system (Table 1).

For the first time our work demonstrates the feasibility of *in vivo* quantification and visualization of human visual pathways at high spatial resolution on 3T in clinically acceptable scan time. We also showed the ability to quantify the tract volume and corresponding diffusion tensor metrics of optic tract and optic radiations as well as distinguishing the optic radiations from the major neighboring pathways such as the ILF, IFOF, OPT and PTR. The middle longitudinal fasciculus is another association tract coursing above the ILF and connecting the temporal lobe with inferior parieto-occipital confluence (not shown) which was discussed in detail elsewhere [61]. Distinguishing the adjacent connections of the occipital cortex is valuable to unravel the neural network of complex visual functions. For example, distinguishing the OPT will be beneficial in the study of visuomotor coordination involving the occipito-ponto-cerebellar tracts [62].

Our DTI acquisition protocol applied high spatial resolution and thinner slice thickness using higher magnetic field strength that resulted in reduction in both partial volume averaging in the voxel and magnetic field gradients. This provided higher and more detectable tensor anisotropy within deep gray matter nuclei such as the LGN [4. It allowed us to trace the optic tract and optic radiation synapsing in the thalamus. The current MRI data were acquired using anisotropic voxel dimensions (i.e., 2 x 2 x 1 mm interpolated in k-space to 1 x 1 x 1 mm). In our experience [48, 61, 22], the acquisition protocol and analysis strategy were adequate for tracing the fibers coursing along the direction of higher resolution (craniocaudally oriented fibers running along the thinner dimension in the axial plane). This acquisition paradigm also resulted in less contamination from craniocaudally oriented crossing fibers within the voxel and less intravoxel inhomogeneity with resultant improved resolution and traceability of fibers running along other dimensions (for example, the visual pathways coursing in the anterior-posterior direction). For example, the current data also enabled the tracing of finer pretectal fibers (Fig. 3f) and the arching route of the Meyer's loop (Figs. 3a) [7].

Using high-resolution 3D fiber tract reconstruction has several advantages over studying 2D ROIs. First, unlike 2D ROI placement, 3D DTT has a better ability to demonstrate the integrity of the fiber tracts by lesions [11, 12, 13]. Second, combining high spatial resolution and smaller slice thickness 3D tractography with cMRI data increases the validity of results obtained from 3D fiber reconstruction. Third, by using multiple ROIs in different planes (sagittal and coronal) contamination and partial volume effects from adjacent tracts, for example, the PTR or OPT was avoided. We delineated the ORs from adjacent major fiber

tracts such as the IFOF, ILF, OPT and PTR which have been a major source of confusion in the occipital lobe on prior DTI studies.

Our quantitative analysis demonstrates a left-sided laterality of the FA values of the optic radiations. This has been reported in prior DTI studies and might be due to developmental asymmetry of the optic radiations, the significance of which remains unclear. All 5 study subjects were right-handed young adult males. However, dominant eye sidedness was not investigated in our subjects which might have a role in the laterality trends of the visual pathways. The number of subjects used in the current study is small to arrive at a more comprehensive quantitative assessment of the effects of side, gender and age. Our results also demonstrate a marked difference in mean diffusivity between the optic tract and optic radiations (MD is markedly higher in optic tract ~ 1.25×10^{-3} mm^2/sec compared to the optic radiation ~ 0.86×10^{-3} mm^2/sec). Since the MD values differ due to the level of CSF-contamination, mean diffusivity is expected to be greater more anteriorly and it is expected to be lower in the posterior structures with lower CSF contamination [10]. To our knowledge, ours is the first tractography study measuring the diffusion tensor metrics of the optic tract volume. Future studies with greater number of subjects will be required to study covariates such as age gender.

In the current study, we used SENSE imaging and reduced echo time < 60ms and opted for a b-factor of 500 to acquire as many thin slices as possible (# 120) to cover the whole brain. One method to reduce susceptibility artifact is using conventional fast spin-echo imaging which is time-consuming for clinical scans requiring full brain coverage. Other strategies have also been attempted including line scans [63], multi-shot EPI, simulated echo, and propeller [10]. At 3.0 T, the air-tissue susceptibility inhomogeneity is most problematic for delineation of the optic nerve especially using thick slices [4]. We applied thinner slices, co-aligned and averaged the data to meet a working SNR_0 of ~ 25 to avoid SNR-related estimation biases [48, 21].

Although, improved resolution was applied in the current study, lack of adequate spatial resolution remains the major limitation of the DTI based tractography in general and to this study in specific [22]. Applying higher spatial resolution reduced some of the challenges regarding to crossing fibers and susceptibility artifacts encountered in the prior studies. This helped avoiding false positive or false negative results and revealed the delicate structure of the optic tract and chiasm and the subcomponents such as the pretectal fibers. However, illustration of the unilateral crossing and non-crossing fibers at the optic chiasm was also attempted in our study but found to be beyond our spatial resolution limit. Applying higher resolution will benefit the ability to resolve the fine course of the noncrossing neurons to the ipsilateral eye as well as the course of the crossing neurons to the contralateral eye at the optic chiasm. The study by Hofer el al. [6] reported that they were able to trace the crossing and noncrossing fibers at the optic chiasm. By observing the course of the fibers in their work, there is a good chance that some of their results are false positive due to the limited spatial resolution. Future advances in MR DTI acquisition techniques with higher spatial resolution may resolve some of the challenges related to the crossing fiber and susceptibility artifacts.

The ability to identify and delineate the Meyer's loop is particularly important in neurosurgical interventions to the temporal lobe, currently used as a treatment for pharmaco-resistant temporal lobe epilepsies. Since normal variations of the Meyer's loop anatomy have been reported in prior studies [2, 14, 64], knowledge of the exact extension of the Meyer's loop is essential to avoid post-operative visual deficit following temporal lobectomy.

Clinically, our preliminary results have the potential to be combined with functional assessments of the visuomotor performance to study and model injury progression (i.e. Wallerian degeneration) due to traumatic or ischemic insults, demyelinating disease and tumors involving the visual pathways which will certainly advance our understanding of the pathogenesis of various disease processes affecting the delicate and vulnerable human visual system. Our study paves the way to future trails to explore recovery and repair due to intervention and training to utilize dormant brain tissue connectivity and neuroplasticity [65].

Conclusions

The current study demonstrated for the first time the feasibility of tracing the delicate visual pathways, including the optic tracts and pretectal fibers as well as major neighboring fiber pathways. We also quantified the volumes and corresponding diffusion tensor metrics of the various segments of visual tracts with clinically feasible scan times.

Acknowledgments

References

1. Tamraz JC, Outin-Tamraz C, Saban R. MR imaging anatomy of the optic pathways. Radiol Clin North Am. 1999; 37:1–36. ix. [PubMed: 10026727]

2. Bürgel U, Schormann T, Schleicher A, Zilles K. Mapping of histologically identified long fiber tracts in human cerebral hemispheres to the MRI volume of a reference brain: position and spatial variability of the optic radiation. Neuroimage. 1999; 10:489–499. [PubMed: 10547327]

3. Choi C, Rubino PA, Fernandez-Miranda JC, Abe H, Rhoton AL. Meyer's loop and the optic radiations in the transsylvian approach to the mediobasal temporal lobe. Neurosurgery. 2006; 59:228–36.

4. Barker GJ. Diffusion-weighted imaging of the spinal cord and optic nerve. J Neurol Sci. 2001; 1:S45–9. Review. [PubMed: 11334989]

5. Xu J, Sun SW, Naismith RT, Snyder AZ, Cross AH, Song SK. Assessing optic nerve pathology with diffusion MRI: from mouse to human. NMR Biomed. 2008; 21:928–40. [PubMed: 18756587]

6. Hofer S, Karaus A, Frahm J. Reconstruction and dissection of the entire human visual pathway using diffusion tensor MRI. Front Neuroanat. 2010; 4:15. [PubMed: 20428499]

7. Mandelstam SA. Challenges of the anatomy and diffusion tensor tractography of the Meyer loop. AJNR Am J Neuroradiol. 2012; 33:1204–1210. [PubMed: 22422189]

8. Lilja Y, Ljungberg M2, Starck G3, Malmgren K4, Rydenhag B5, Nilsson DT6. Visualizing Meyer's loop: A comparison of deterministic and probabilistic tractography. Epilepsy Res. 2014; 108:481–90. [PubMed: 24559840]

9. Iwasawa T1, Matoba H, Ogi A, Kurihara H, Saito K, Yoshida T, Matsubara S, Nozaki A. Diffusion-weighted imaging of the human optic nerve: a new approach to evaluate optic neuritis in multiple sclerosis. Magn Reson Med. 1997; 38:484–91. [PubMed: 9339450]

10. Ueki S, Fujii Y, Matsuzawa H, Takagi M, Abe H, Kwee IL, Nakada T. Assessment of axonal degeneration along the human visual pathway using diffusion trace analysis. Am J Ophthalmol. 2006; 142:591–96. [PubMed: 17011850]

11. Conturo TE1, Lori NF, Cull TS, Akbudak E, Snyder AZ, Shimony JS, McKinstry RC, Burton H, Raichle ME. Tracking neuronal fiber pathways in the living human brain. Proc Natl Acad Sci U S A. 1999; 96:10422–7. [PubMed: 10468624]

12. Mori S, Kaufmann WE, Davatzikos C, Stieltjes B, Amodei L, Fredericksen K, Pearlson GD, Melhem ER, Solaiyappan M, Raymond GV, Moser HW, van Zijl PC. Imaging cortical association tracts in the human brain using diffusion-tensor-based axonal tracking. Magn Reson Med. 2002; 47:215–23. [PubMed: 11810663]

13. Catani M, Jones DK, Donato R, Ffytche DH. Occipito-temporal connections in the human brain. Brain. 2003; 126(Pt 9):2093–107. [PubMed: 12821517]

14. Yamamoto T, Yamada K, Nishimura T, Kinoshita S. Tractography to depict three layers of visual field trajectories to the calcarine gyri. Am J Ophthalmol. 2005; 140:781–85. [PubMed: 16310456]

15. Toosy AT1, Ciccarelli O, Parker GJ, Wheeler-Kingshott CA, Miller DH, Thompson AJ. Characterizing function-structure relationships in the human visual system with functional MRI and diffusion tensor imaging. Neuroimage. 2004; 21:1452–63. [PubMed: 15050570]

16. Staempfli P, Rienmueller A, Reischauer C, Valavanis A, Boesiger P, Kollias S. Reconstruction of the human visual system based on DTI fiber tracking. J Magn Reson Imaging. 2007; 26:886–93. [PubMed: 17896363]

17. Clatworthy PL, Williams GB, Acosta-Cabronero J, Jones SP, Harding SG, Johansen-Berg H, Baron JC. Probabilistic tractography of the optic radiations--an automated method and anatomical validation. Neuroimage. 2010; 49:2001–12. [PubMed: 19900564]

18. Kolbe S, Chapman C, Nguyen T, Bajraszewski C, Johnston L, Kean M, Mitchell P, Paine M, Butzkueven H, Kilpatrick T, Egan G. Optic nerve diffusion changes and atrophy jointly predict visual dysfunction after optic neuritis. Neuroimage. 2009; 45:679–86. [PubMed: 19162205]

19. Vinogradov E1, Degenhardt A, Smith D, Marquis R, Vartanian TK, Kinkel P, Maier SE, Hackney DB, Lenkinski RE. High-resolution anatomic, diffusion tensor, and magnetization transfer magnetic resonance imaging of the optic chiasm at 3T. Magn Reson Imaging. 2005; 22:302–6.

20. Sarlls JE, Pierpaoli C. In vivo diffusion tensor imaging of the human optic chiasm at sub-millimeter resolution. Neuroimage. 2009; 47:1244–1251. [PubMed: 19520170]

21. Wargo CJ, Gore JC. Localized high-resolution DTI of the human midbrain using single-shot EPI, parallel imaging, and outer-volume suppression at 7T. Magn Reson Imaging. 2013; 31:810–19. [PubMed: 23541390]

22. Polonara G1, Salvolini S, Fabri M, Mascioli G, Cavola GL, Neri P, Mariotti C, Giovannini A, Salvolini U. Unilateral visual loss due to ischaemic injury in the right calcarine region: a functional magnetic resonance imaging and diffusion tension imaging follow-up study. Int Ophthalmol. 2011; 31:129–34. [PubMed: 21293901]

23. Frohman EM1, Dwyer MG, Frohman T, Cox JL, Salter A, Greenberg BM, Hussein S, Conger A, Calabresi P, Balcer LJ, Zivadinov R. Relationship of optic nerve and brain conventional and non-conventional MRI measures and retinal nerve fiber layer thickness, as assessed by OCT and GDx: a pilot study. J Neurol Sci. 2009; 282:96–105. [PubMed: 19439327]

24. Reich DS, Smith SA, Gordon-Lipkin EM, Ozturk A, Caffo BS, Balcer LJ, Calabresi PA. Damage to the optic radiation in multiple sclerosis is associated with retinal injury and visual disability. Arch Neurol. 2009; 66:998–1006. [PubMed: 19667222]

25. Kolappan M, Henderson AP, Jenkins TM, Wheeler-Kingshott CA, Plant GT, Thompson AJ, Miller DH. Assessing structure and function of the afferent visual pathway in multiple sclerosis and associated optic neuritis. J Neurol. 2009; 256:305–19. [PubMed: 19296047]

26. Naismith RT, Xu J, Tutlam NT, Trinkaus K, Cross AH, Song SK. Radial diffusivity in remote optic neuritis discriminates visual outcomes. Neurology. 2010; 74:1702–10. [PubMed: 20498438]

27. Rueda Lopes FC1, Doring T, Martins C, Cabral FC, Malfetano FR, Pereira VC, Alves-Leon S, Gasparetto EL. The role of demyelination in neuromyelitis optica damage: diffusion-tensor MR imaging study. Radiology. 2012; 263(1):235–42. [PubMed: 22438446]

28. Kodl CT, Franc DT, Rao JP, Anderson FS, Thomas W, Mueller BA, Lim KO, Seaquist ER. Diffusion tensor imaging identifies deficits in white matter microstructure in subjects with type 1 diabetes that correlate with reduced neurocognitive function. Diabetes. 2008; 57:3083–9. [PubMed: 18694971]

29. Garaci FG, Bolacchi F, Cerulli A, Melis M, Spano A, Cedrone C, Floris R, Simonetti G, Nucci C. Optic nerve and optic radiation neurodegeneration in patients with glaucoma: in vivo analysis with 3-T diffusion-tensor MR imaging. Radiology. 2009; 252:496–501. [PubMed: 19435941]

30. Engelhorn T, Michelson G, Waerntges S, Struffert T, Haider S, Doerfler A. Diffusion tensor imaging detects rarefaction of optic radiation in glaucoma patients. Acad Radiol. 2011; 18:764–9. [PubMed: 21377906]

31. Wang MY1, Wu K, Xu JM, Dai J, Qin W, Liu J, Tian J, Shi D. Quantitative 3-T diffusion tensor imaging in detecting optic nerve degeneration in patients with glaucoma: association with retinal nerve fiber layer thickness and clinical severity. Neuroradiology. 2013; 55:493–8. [PubMed: 23358877]

32. Xie S, Gong GL, Xiao JX, Ye JT, Liu HH, Gan XL, Jiang ZT, Jiang XX. Underdevelopment of optic radiation in children with amblyopia: a tractography study. Am J Ophthalmol. 2007; 143:642–6. [PubMed: 17276381]

33. Shimony JS, Burton H, Epstein AA, McLaren DG, Sun SW, Snyder AZ. Diffusion tensor imaging reveals white matter reorganization in early blind humans. Creb Cortex. 2006; 16:1653–61.

34. Shu N, Li J, Li K, Yu C, Jiang T. Abnormal diffusion of cerebral white matter in early blindness. Hum Brain Mapp. 2009; 30:220–27. [PubMed: 18072278]

35. Thomas B, Eyssen M, Peeters R, Molenaers G, Van Hecke P, De Cock P, Sunaert S. Quantitative diffusion tensor imaging in cerebral palsy due to periventricular white matter injury. Brain. 2005; 128:2562–77. [PubMed: 16049045]

36. Rosiene J, Liu X, Imielinska C, Ferrera J, Bruce J, Hirsch J, D'Ambrosio A. Structure-function relationships in the human visual system using DTI, fMRI and visual field testing: pre- and post-operative assessments in patients with anterior visual pathway compression. Stud Health Technol Inform. 2006; 119:464–6. [PubMed: 16404100]

37. Salmela MB, Cauley KA, Andrews T, Gonyea JV, Tarasiewicz I, Filippi CG. Magnetic resonance diffusion tensor imaging of the optic nerves to guide treatment of pediatric suprasellar tumors. Pediatr Neurosurg. 2009; 45:467–71. [PubMed: 20110761]

38. Chen X, Weigel D, Ganslandt O, Buchfelder M, Nimsky C. Prediction of visual field deficits by diffusion tensor imaging in temporal lobe epilepsy surgery. Neuroimage. 2009; 45:286–97. [PubMed: 19135156]

39. Coenen VA, Huber KK, Krings T, Weidemann J, Gilsbach JM, Rohde V. Diffusion-weighted imaging-guided resection of intracerebral lesions involving the optic radiation. Neurosurg Rev. 2005; 28:188–95. [PubMed: 15747136]

40. Ebeling U, Reulen HJ. Neurosurgical topography of the optic radiation in the temporal lobe. Acta Neurochir (Wien). 1988; 92:29–36. [PubMed: 3407471]

41. Yasargil MG, Türe U, Yasargil DHC. Impact of temporal lobe surgery. J Neurosurg. 2004; 101:725–738. [PubMed: 15540909]

42. Powell HW, Parker GJ, Alexander DC, Symms MR, Boulby PA, Wheeler-Kingshott CA, Barker GJ, Koepp MJ, Duncan JS. MR tractography predicts visual field defects following temporal lobe resection. Neurology. 2005; 65:596–9. [PubMed: 16116123]

43. Winston GP, Yogarajah M, Symms MR, McEvoy AW, Micallef C, Duncan JS. Diffusion tensor imaging tractography to visualize the relationship of the optic radiation to epileptogenic lesions prior to neurosurgery. Epilepsia. 2011; 52:1430–8. [PubMed: 21569018]

44. Anik I, Anik Y, Koc K, Ceylan S, Genc H, Altintas O, Ozdamar D, Baykal Ceylan D. Evaluation of early visual recovery in pituitary macroadenomas after endoscopic endonasal transphenoidal surgery: Quantitative assessment with diffusion tensor imaging (DTI). Acta Neurochir (Wien). 2011; 153:831–42. [PubMed: 21267606]

45. Schoth F, Krings T. Diffusion-tensor imaging in septo-optic dysplasia. Neuroradiology. 2004; 46:759–63. [PubMed: 15160259]

46. Salmela MB, Cauley KA, Nickerson JP, Koski CJ, Filippi CG. Magnetic resonance diffusion tensor imaging (MRDTI) and tractography in children with septo-optic dysplasia. Pediatr Radiol. 2010–40:708–13.

47. Alexander AL, Hasan KM, Lazar M, Tsuruda JS, Parker DL. Analysis of partial volume effects in diffusion-tensor MRI. Magn Reson Med. 2001; 45:770–80. [PubMed: 11323803]

48. Hasan KM, Kamali A, Kramer LA. Mapping the human brain white matter tracts relative to cortical and deep gray matter using diffusion tensor imaging at high spatial resolution. Magn Reson Imaging. 2009; 27:631–6. [PubMed: 19128910]

49. Hasan KM, Halphen C, Boska MD, Narayana PA. Diffusion tensor metrics, T2 relaxation, and volumetry of the naturally aging human caudate nuclei in healthy young and middle-aged adults: possible implications for the neurobiology of human brain aging and disease. Magn Reson Med. 2008; 59:7–13. [PubMed: 18050345]

50. Kramer LA, Sargsyan AE, Hasan KM, Polk JD, Hamilton DR. Orbital and intracranial effects of microgravity: findings at 3-T MR imaging. Radiology. 2012; 263:819–27. [PubMed: 22416248]

51. Hasan KM, Narayana PA. Computation of the fractional anisotropy and mean diffusivity maps without tensor decoding and diagonalization: Theoretical analysis and validation. Magn Reson Med. 2003; 50:589–98. [PubMed: 12939767]

52. Mori S, van Zijl PC. Fiber tracking: principles and strategies - a technical review. NMR Biomed. 2002; 15:468–80. [PubMed: 12489096]

53. Filley CM. White matter and behavioral neurology. Ann N Y Acad Sci. 2005; 1064:162–83. Review. [PubMed: 16394155]

54. Hasan KM, Halphen C, Sankar A, Eluvathingal TJ, Kramer L, Stuebing KK, Ewing-Cobbs L, Fletcher JM. Diffusion tensor imaging-based tissue segmentation: validation and application to the developing child and adolescent brain. Neuroimage. 2007; 34:1497–505. [PubMed: 17166746]

55. Hains, DE. An Atlas of Structures, Sections and Systems. 7. New York: Lippincott Williams & Wilkins; 2007. Neuroanatomy.

56. Hua K, Zhang J, Wakana S, Jiang H, Li X, Reich DS, Calabresi PA, Pekar JJ, van Zijl PC, Mori S. Tract probability maps in stereotaxic spaces: analyses of white matter anatomy and tract-specific quantification. Neuroimage. 2008; 39:336–47. [PubMed: 17931890]

57. Kamali A, Kramer LA, Frye RE, Butler IJ, Hasan KM. Diffusion tensor tractography of the human brain cortico-ponto-cerebellar pathways: a quantitative preliminary study. J Magn Reson Imaging. 2010; 32:809–17. [PubMed: 20882611]

58. Tao XF, Wang ZQ, Gong WQ, Jiang QJ, Shi ZR. A new study on diffusion tensor imaging of the whole visual pathway fiber bundle and clinical application. Chin Med J (Engl). 2009; 122:178–82. [PubMed: 19187643]

59. Yamamoto A, Miki Y, Urayama S, Fushimi Y, Okada T, Hanakawa T, Fukuyama H, Togashi K. Diffusion tensor fiber tractography of the optic radiation: analysis with 6-, 12-, 40-, and 81-directional motion-probing gradients, a preliminary study. AJNR Am J Neuroradiol. 2007; 28:92–96. [PubMed: 17213432]

60. Yamada M, Momoshima S, Masutani Y, Fujiyoshi K, Abe O, Nakamura M, Aoki S, Tamaoki N, Okano H. Diffusion-tensor neuronal fiber tractography and manganese-enhanced MR imaging of primate visual pathway in the common marmoset: preliminary results. Radiology. 2008; 249:855–64. [PubMed: 19011185]

61. Kamali A, Flanders AE, Brody J, Hunter JV, Hasan KM. Tracing superior longitudinal fasciculus connectivity in the human brain using high resolution diffusion tensor tractography. Brain Struct Funct. 2014; 219:269–81. [PubMed: 23288254]

62. Kamali A, Kramer LA, Hasan KM. Feasibility of prefronto-caudate pathway tractography using high resolution diffusion tensor tractography data at 3T. J Neurosci Methods. 2010; 191:249–54. [PubMed: 20600311]

63. Mamata H, Mamata Y, Westin CF, Shenton ME, Kikinis R, Jolesz FA, Maier SE. High-resolution line scan diffusion tensor MR imaging of white matter fiber tract anatomy. AJNR Am J Neuroradiol. 2002; 23:67–75. [PubMed: 11827877]

64. Sherbondy AJ, Dougherty RF, Napel S, Wandell BA. Identifying the human optic radiation using diffusion imaging and fiber tractography. J Vis. 2008; 8:12.1–11. [PubMed: 19146354]

65. Thiagarajan P, Ciuffreda KJ, Capo-Aponte JE, Ludlam DP, Kapoor N. Oculomotor neurorehabilitation for reading in mild traumatic brain injury (mTBI): An integrative approach. NeuroRehabilitation. 2014; 34:129–46. [PubMed: 24284470]
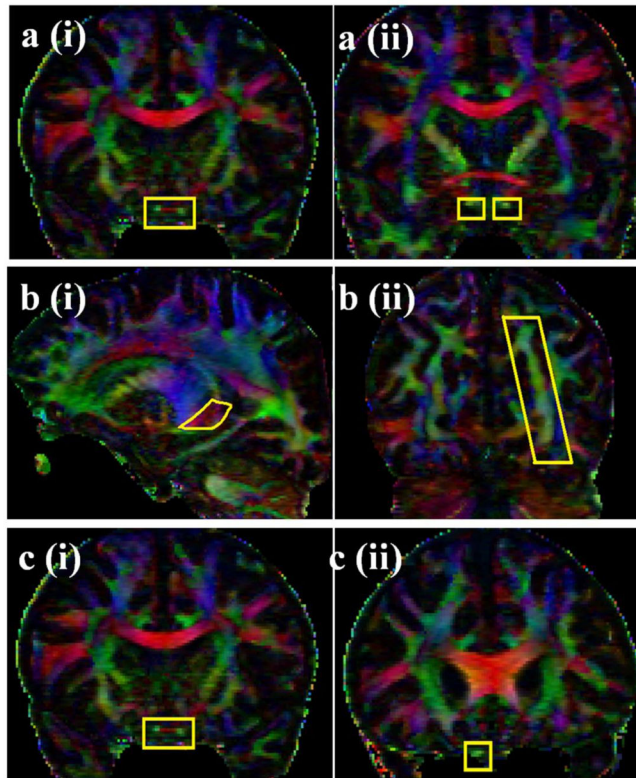
Figure 1.
The selected ROI seeds (ROI 1 and ROI 2) for optic tract and optic radiation are illustrated on the coronal DTI color-coded map. To trace the OT, the first ROI was placed over the optic chiasm in the coronal plane (1ai). The second ROI was pursued by selecting the anterior-posterior oriented green association fibers shown in the coronal plane passing through the level of the anterior commissure (Fig. 1aii). The first ROI to trace the OR was seeded on the red fibers of the thalamus (1bi) (right to left oriented fibers that loop over the temporal horn of lateral ventricle before turning medially toward the calcarine sulcus in the occipital lobe). The second ROI was pursued on the green fibers (anterior-posteriorly oriented fibers) in the occipital cortex (Fig. 1bii). The ROIs for delineation of the optic nerve are seen in Fig. 1ci and 1 cii. The first ROI was placed over the optic chiasm in the coronal plane (1ci). The second ROI was placed on the optic nerve at the level of the rostrum of the corpus collosum on the coronal plane.
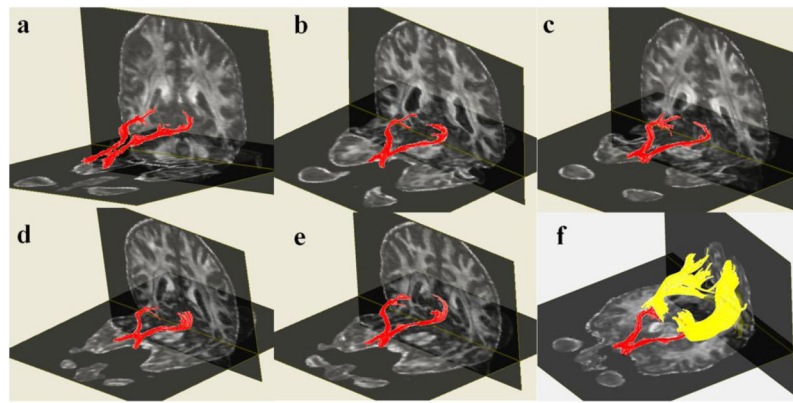
Figure 2.
Three-dimensional reconstructions of the optic chiasm and optic tracts created for five subjects are shown (2a–e). Optic radiations are also illustrated for subject number five (2f).
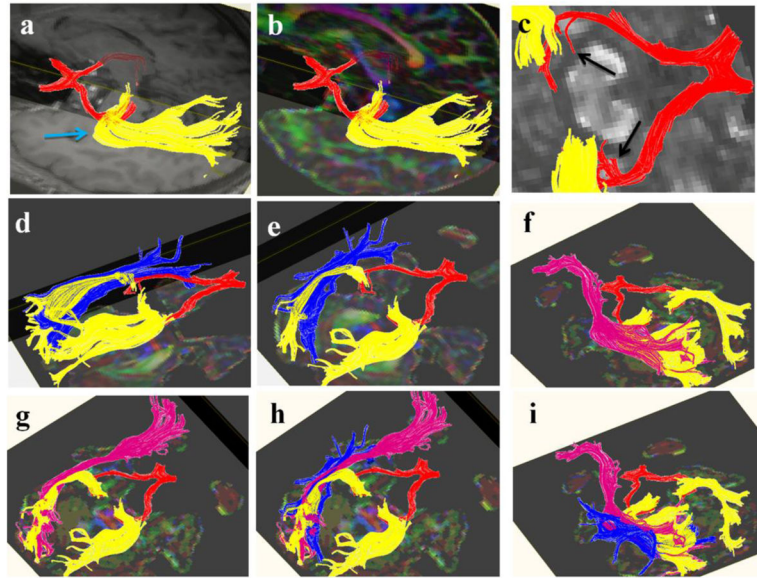
Figure 3.
Three-dimensional reconstructions of the optic chiasm, optic tract (in red) and optic radiations (in yellow) are illustrated (3a–c). Adjacent pathways such as the ILF (blue) and IFOF (pink) are also illustrated (3d–i). The Meyer's loop is annotated by a blue arrow in 3a. The pretectal branches of the optic tract are shown by black arrows in 3c. As shown in 3d–i, the optic radiations are covered by the IFOF and both are overlapped by the ILF (3h–i) along their course through the temporo-occipital white matter.
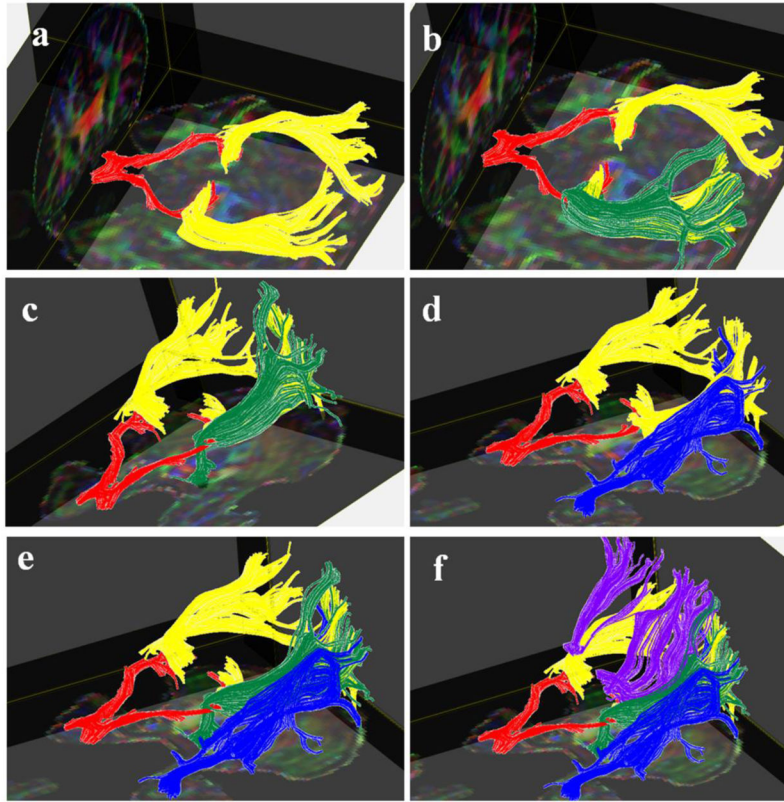
Figure 4.
Representative 3D tractogram of the optic tract (red), optic radiation (yellow) and their association with adjacent fiber tracts such as the OPT (green), ILF (blue) and PTR (purple) in one of the subjects. As shown in 4b–c, the OPT is also covering the optic radiation and both are overlapped by the ILF during their course toward the occipital cortex (4d–e). The PTR (purple fibers) course above the optic radiations and insert into the parieto-occipital cortices (4f).

Table 1

A quantitative summary of the mean and standard deviation values of fiber tract volume and corresponding fractional anisotropy (FA) and mean diffusivity (MD) the bilateral optic radiations (OR) and optic tracts (OT).

Healthy Males (N=5)	Volume (mL)	FA	MD (x 10^{-3} mm^2 sec^{-1})
Optic Radiations (Right)	6.954 ± 1.905	0.478 ± 0.031	0.860 ± 0.036
Optic Radiations (Left)	5.972 ± 2.247	0.497 ± 0.027	0.867 ± 0.033
OR (Right and Left)	12.926 ± 3.718	0.486 ± 0.027	0.866 ± 0.033
p (R vs. L)	0.31	**0.06**	0.37
Optic tract	2.052 ± 0.315	0.477 ± 0.028	1.253 ± 0.045
P (OR vs. OT)	<0.001	0.48	**0.00004**
Whole Brain White Matter	777.92 ± 72.25		